Transonic, Turbulent Boundary-Layer Separation Generated on an Axisymmetric Flow Model

W. D. Bachalo*
Aerometrics Inc., Mountain View, California
and
D. A. Johnson*
NASA Ames Research Center, Moffett Field, California

Experimental data describing the transonic, turbulent, separated flow generated by an axisymmetric flow model are presented. The model consisted of a circular-arc bump affixed to a straight, circular cylinder aligned with the flow direction. Measurements of the mean velocity, turbulence intensity, and Reynolds shear-stress profiles were made in the separated flow. These data revealed dramatic changes in the shear-stress levels as the flow passed through the interaction to reattachment. Behavior of the turbulence reaction to the imposed pressure gradients was examined in terms of the mixing length and the excursions of the turbulence from equilibrium.

Nomenclature

c = chord length of the bump
C_f = skin friction velocity, $\tau_w/\frac{1}{2}u_e$
C_P = surface pressure coefficient, $(p-p_\infty)/\frac{1}{2}\rho_\infty u_\infty^2$
H = shape parameter, δ_1/δ_2
ℓ = mixing length
M = Mach number
M_P = Mach number, peak value
M_∞ = Mach number, freestream conditions
u = mean velocity component in the streamwise direction
$\langle u' \rangle$ = streamwise turbulence intensity
u_τ = wall friction velocity, $=\sqrt{\tau_w/\rho}$
v = mean velocity component in the normal direction
$\langle v' \rangle$ = normal turbulence intensity
x,y = coordinates in the streamwise and normal directions, respectively
β_p = pressure gradient parameter, $= -\delta_2 dp/\rho_e u_e^2 dx$
δ = thickness of the viscous layer
δ_1,δ_2 = displacement and momentum thicknesses, respectively, of the viscous layer
θ = flow angle, $=\arctan(v/u)$
θ_m = local slope of the model surface
θ_δ = slope of the boundary-layer contour, $=\arctan(\Delta\delta/\Delta x)$
θ_{δ_1} = slope of the displacement thickness contour, $=\arctan(\Delta\delta/\Delta x)$

Introduction

THE ultimate performance of fluid machinery such as turbines, jet engines, and compressors, as well as wings and helicopter rotors, is dictated by stalling or separation of the boundary layer. Hence, it is imperative that prediction methods be developed for these flows. At transonic speeds, the flows are especially difficult to predict because of the strong viscous-inviscid interactions. Successful prediction of such flows has been hampered by the weakness of existing turbulence closure models. Although a number of mathematical models for predicting turbulent flows have been developed[1] that vary in complexity and in their ability to predict the flows, none of the models satisfactorily predict flows that are subjected to an adverse pressure gradient which leads to massive separation. Attempts at predicting the flows are partially frustrated by the existence of the nonequilibrium effects introduced through the interaction. Reliable experimental data were required for the development and evaluation of the computational schemes.

Several papers have been published describing the experimental investigation of transonic, turbulent, boundary-layer separation.[2-5] Alber et al.[2] used a floor-mounted, two-dimensional bump model to generate the transonic flowfield. Oil-flow visualization showed that the surface flow was subject to some three-dimensional effects. The slow-moving flow near the wall can easily move laterally when subjected to an adverse pressure gradient. The use of a floor-mounted model also has the difficulty of obtaining the scaled bump height to incident boundary-layer thickness without causing choking of the wind tunnel.

In Ref. 4, measurements were made in the rear portion of the transonic flow over a circular-arc airfoil using a laser velocimeter. The investigation showed that the maximum turbulent kinetic energy and shear stress occurred at a location where the maximum normal velocity gradient also occurred, thus demonstrating the possibility of using a scalar eddy-viscosity model. Measurements on an NACA 64A010[5] airfoil produced data in remarkable agreement with the Escudier mixing-length model on the downstream part of the separated region. The results suggested that the difficulty in predicting such flows may be due to the inability of the turbulence models to describe the flow development near the separation point. This region requires further experimental investigation if improved predictions of the flow separation are to be achieved.

In the present work, an attempt was made to isolate some of the fundamental features of the flow and measure these phenomena in detail. An axisymmetric flow model, which provided a high-quality flowfield free from wall interference, three-dimensional effects, and excessive unsteadiness, was developed for this purpose. The geometry also proved to be well suited for measurements with the laser velocimeter.

Some preliminary measurements were made and reported in Ref. 6. Since that time, the laser velocimeter has been developed to provide simultaneous two-velocity component

Presented as Paper 79-1479 at the AIAA 12th Fluid and Plasma Dynamics Conference, Willamsburg, VA, July 24-26, 1979; received Aug. 27, 1984; revision received July 1, 1985.

*Research Scientist. Member AIAA.

measurements, each having the necessary frequency shifting. Streamwise and normal mean velocities, turbulence intensities, and Reynolds shear stress have been measured. These data are reported here along with a discussion of the results. The complete set of data obtained during this experiment is available in Ref. 7.

Experimental Apparatus and Test Conditions

Transonic Flow Model

The experiments were conducted in the NASA Ames Research Center 2×2 ft Transonic Wind Tunnel. This facility is a closed-return, variable-density, continuous-running tunnel with 21% open, porous-slotted upper and lower walls.

An axisymmetric flow model designed for this investigation consisted of an annular circular-arc bump affixed to a circular cylinder aligned with the flow direction, see Fig. 1. The thin-walled cylinder was 15.2 cm in outside diameter and extended 61 cm upstream of the bump's leading edge. A straight, smooth finish on the cylinder was ensured by careful grinding of the surface. The straight section of the cylinder permitted natural transition to a fully turbulent boundary layer at a Reynolds number of 13.2×10^6/m at the interaction. The boundary layer incident on the bump was of sufficient thickness (~1 cm) to allow accurate determination of the boundary-layer information. However, in comparison to the interaction observed on airfoils, the boundary layer was not so thick as to give rise to a separation of greater severity than is representative of full scale. The boundary-layer thickness was also relatively thin compared to the cylinder radius of curvature (~1:7.6) so that predictions for two-dimensional results could be compared with the experimental data.

In the present investigation, a bump of 20.32 cm chord and 1.91 cm thick was used. The leading edge was joined to the cylinder by a smooth circular arc of radius 18.3 cm that was tangent to the cylinder 3.3 cm upstream and to the bump 2.2 cm downstream of the intersection of the arc of the bump with the cylinder.

For the implementation of the laser velocimeter, the model had further advantages. With the curved surfaces, diffuse reflection of the laser beams from the model surface was reduced, allowing measurements to be made very close to the wall (to within 0.2 mm). This was especially advantageous for the measurement of the normal velocity component. By adjusting the off-axis location of the collecting optics, the light scattered by reflection and diffraction of the focused beams from the model surface was avoided.

The axisymmetric configuration was also found to be relatively free from troublesome sidewall interference. Unlike the case of a plane two-dimensional airfoil that spans the test section and thus interacts with the tunnel boundary layers, the shock on the present model terminated before reaching the tunnel wall. As a result, the flow was much steadier than the two-dimensional flows. Furthermore, the shock strength decreased with the inverse square of the distance from the model rather than with the inverse of the distance as for a plane two-dimensional airfoil. Thus, a greater range of freestream Mach numbers (to $M=0.9$) could be used without tunnel blockage or sizeable wall interference.

The Ames 2×2 ft two-component laser Doppler velocimeter and holographic interferometer were described previously in Ref. 5.

Results and Discussion

The data were acquired at a freestream Mach number of $M_\infty=0.875$ and a unit Reynolds number of $Re/\text{m}=13.6\times10^6$. At these conditions, the shock that occurred at a downstream location of $x/c=0.66$ was, in itself, of insufficient strength to produce a separation. However, the combination of the perturbation introduced into the boundary

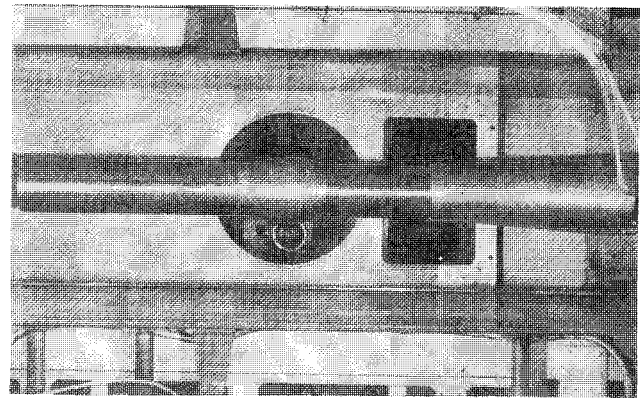

Fig. 1 Axisymmetric transonic flow model.

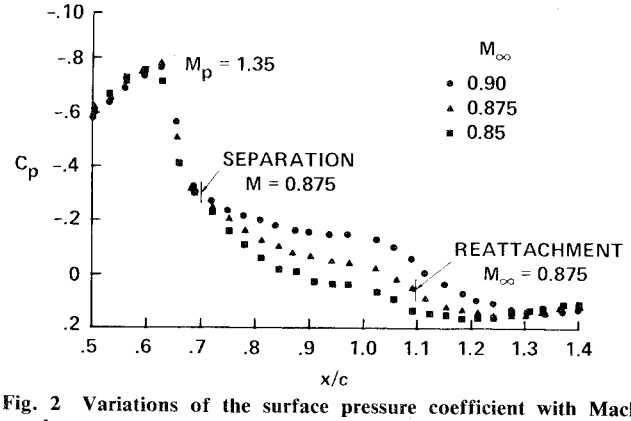

Fig. 2 Variations of the surface pressure coefficient with Mach numbers.

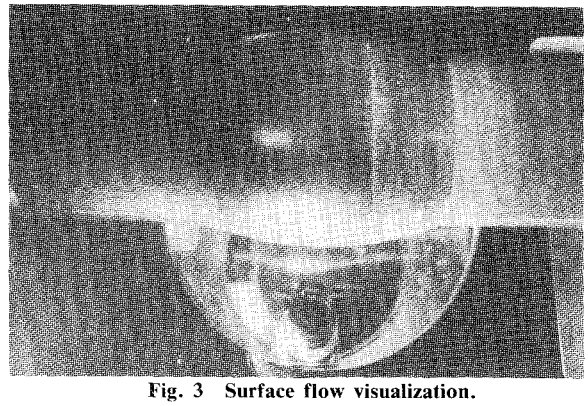

Fig. 3 Surface flow visualization.

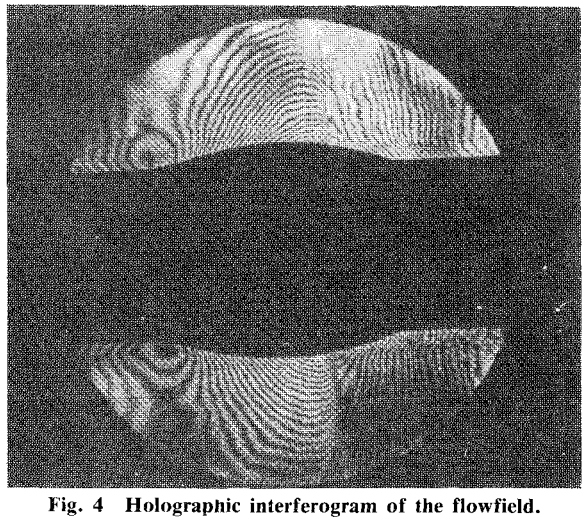

Fig. 4 Holographic interferogram of the flowfield.

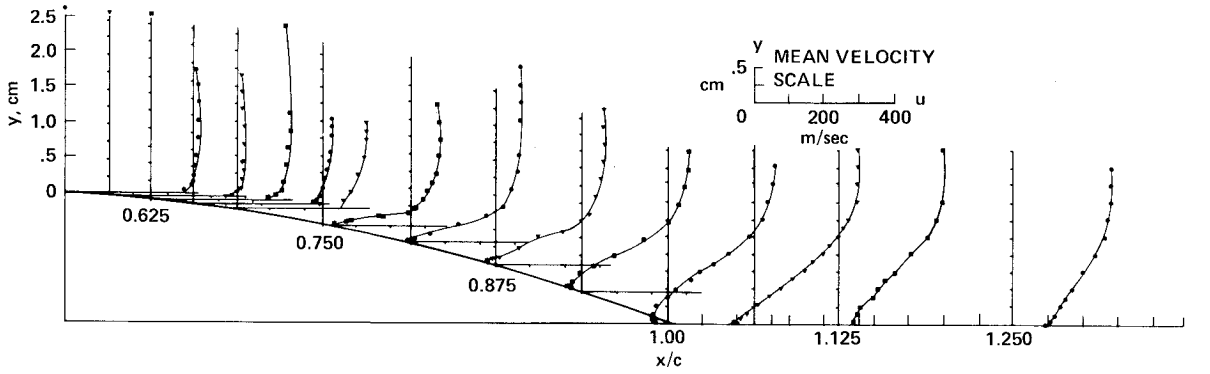

Fig. 5 Mean velocity profiles.

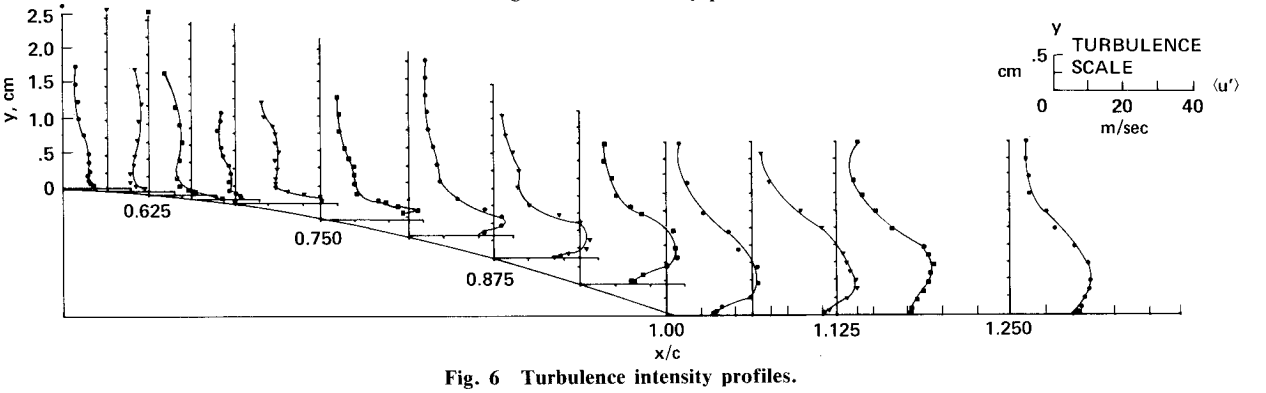

Fig. 6 Turbulence intensity profiles.

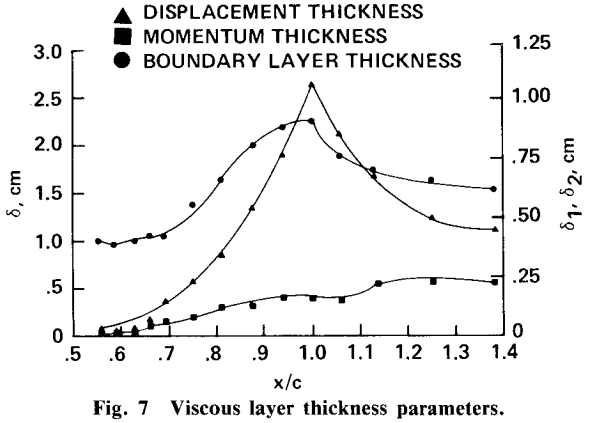

Fig. 7 Viscous layer thickness parameters.

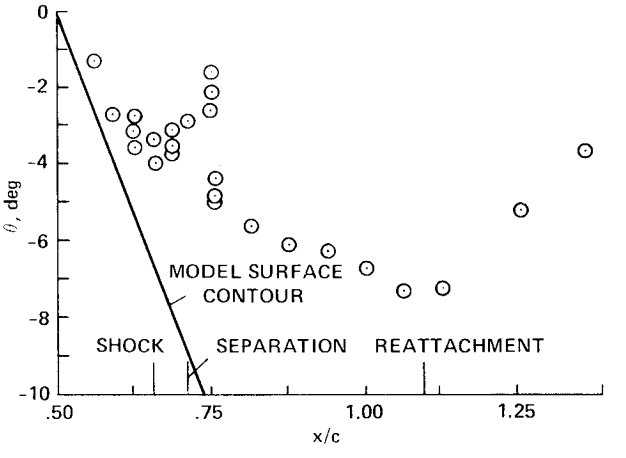

Fig. 8 Flow angle at the outer edge of the viscous layer.

layer by the shock and the trailing-edge gradient caused the flow to separate downstream of the shock at $x/c \cong 0.70$.

Figure 2 reveals the variation in the location and severity of the separation with an incremental change in the Mach numbers. At $M = 0.85$, the shock did not produce a sufficient pressure rise to cause separation. However, pressure gradient separation occurred in the trailing-edge region as can be seen in the change in slope of the pressure curve ($x/c \cong 0.88$) and was confirmed by surface flow visualization. The separation line moved upstream with an increase of the freestream Mach number, $M = 0.875$. A noticeable reduction in the downstream pressure recovery resulted with the progression upstream of the separation line. Increasing the Mach number to $M = 0.90$ caused the separation to move the foot of the shock, which produced an additional reduction in the pressure recovery. For this case, a constant-pressure plateau occurred over a region of the separated flow. The shock location did not show any detectable movement upstream as might have been expected.

A peak Mach number for the freestream condition of $M = 0.875$ computed from the surface pressure was $M_P = 1.31$. $M_P \cong 1.32$ has been suggested as the minimum that will produce a pressure rise sufficient to cause separation. In the present case, the separation was estimated to have occurred slightly downstream of the shock.

Figure 3 shows the surface oil-flow pattern obtained at $M = 0.875$. Flow upstream of the separation can be seen to have been free from any three-dimensional effects, as was the flow in the reversed-flow region.

Inviscid flow visualization was obtained from the holographic interferogram shown in Fig. 4. The flow showed good axial symmetry, as can be seen from the similarity of the flow above and below the model. As a result, the shock appeared as a well-defined plane around the model. The inviscid flow on this model was found to be exceptionally stable. Subsequent tests in the Ames 6×6 ft wind tunnel indicated a similar surface pressure distribution. This agreement alleviated the concern with wind tunnel wall effects on the interaction.

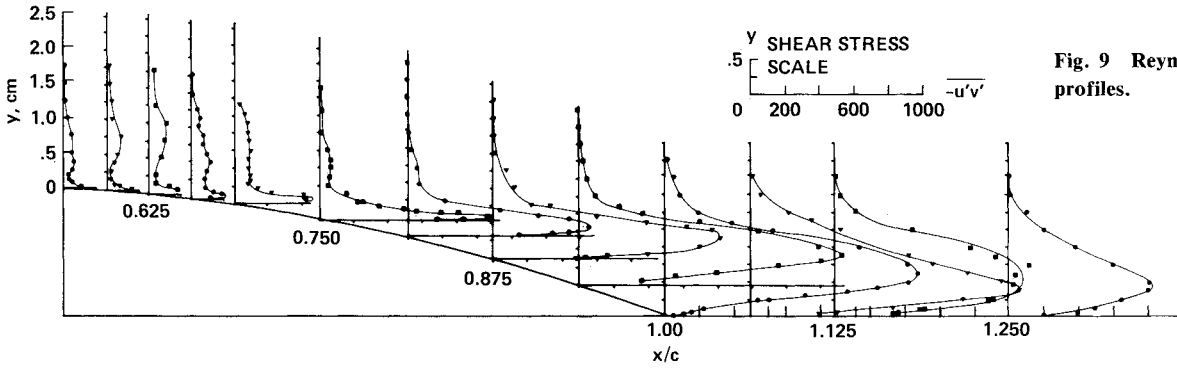

Fig. 9 Reynolds shear-stress profiles.

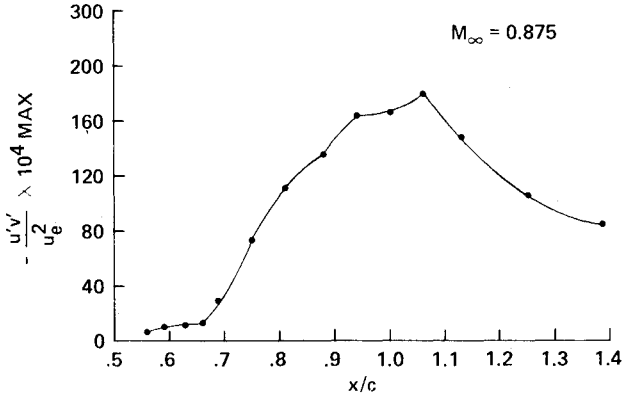

Fig. 10 Distribution of the maximum shear stress.

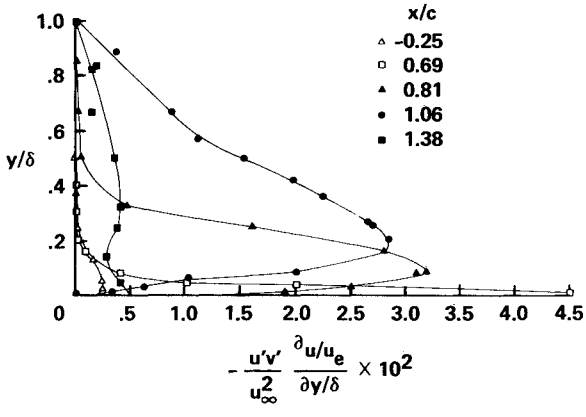

Fig. 11 Turbulence production.

Viscous Flow Properties

Viscous flow properties, which included the mean streamwise and normal velocity profiles, turbulence intensities, and turbulent shear stresses, were measured throughout the interaction region and beyond the flow reattachment. Flow velocity profiles and other turbulence parameters approaching the bump were measured at $x/c = 0.25$ to provide initial conditions for the computational efforts. These data are available in Ref. 7. The acceleration of the flow up the forward half of the bump (Fig. 5) resulted in a decrease in the boundary-layer displacement thickness upstream of the interaction. However, the turbulence intensity levels in the outer part of the boundary layer remained relatively high ($\sim 5\%$), as seen in profile in Fig. 6 at $x/c = 0.56$. At subsequent stations there was a rise in the turbulence intensity in the outer region of the boundary layer as a result of jitter of the compression fan in the neighborhood of the shock. This interaction between the inviscid compression and the turbulent boundary layer caused an apparent increase in the shear stresses.

Approaching the shock/boundary-layer interaction region, the low-momentum flow near the wall was decelerated, which turned the adjacent flow away from the wall. The inviscid flow angle at the boundary-layer edge immediately downstream of the shock ($x/c = 0.68$) was measured to be $\theta \sim 3.5$ deg. This corresponded to a turning angle of 3.6 deg away from the model surface. Alber et al.[2] have claimed that separation cannot occur at the shock until the compression waves formed by the free interaction have turned the flow through an angle of approximately 6.6 deg. They also found that the slope of the measured displacement thickness changed approximately 6 deg in passing the leading foot of the shock in the shock-induced separation mode. In the present case, separation occurred downstream of the shock, but the slope of the δ_1 contour was approximately equal to 6.5 deg.

For pressure gradient separation to be imminent, Alber[9] suggested the following criterion:

$$\beta_p = \frac{\delta_2}{u_e}\frac{du_e}{dx} = \frac{\theta}{\rho_e u^2}\frac{dp}{dx} > 0.004 \qquad (1)$$

An estimate of pressure gradient parameter β_p immediately downstream of the shock was determined to be 0.005. Downstream of separation, β_p dropped to 0.003. Reattachment was found to occur at $\beta_p \sim 0.0065$ (Ref. 9) for both shock-induced and pressure gradient separation. Although the exact location of the reattachment point could not be determined in this investigation, it was estimated to be at $x/c \cong 1.1$. β_p calculated at this station was found to be $\beta_p \cong 0.0062$.

Inspection of the mean velocity profile just downstream of the apparent separation line ($x/c = 0.75$) revealed that the minimum velocity measured was still $u = 30$ m/s. The measurements were made to within 0.2 mm of the wall. However, the viscous sublayer, which separated first, was too thin to be measured with the laser Doppler velocimeter. In the separated region, the maximum measured reversed velocity of $u/u_e = -0.16$ was very close to the value of $u/u_e = -0.15$ measured by Alber et al.[2] for the rear separation case.

The streamwise distributions of the viscous layer thickness and the computed displacement (δ_1) and momentum thickness (δ_2) are displayed in Fig. 7. It can be seen that both the boundary layer and displacement thickness remained approximately constant until the separation line, whereafter they both increased sharply ($\theta \approx 6.6$ deg). These quantities continued to increase up to the trailing edge of the bump. The displacement thickness reached a value of approximately 20 times the value upstream of the interaction. Downstream of the bump trailing edge, the slopes of viscous layer and displacement thickness decreased as the separated flow began the rehabilitation process.

Figure 8 is a plot of the mean flow direction at the outer edge of the viscous layer. The measurements were obtained at a fixed distance of $y = 1.52$ cm from the model surface.

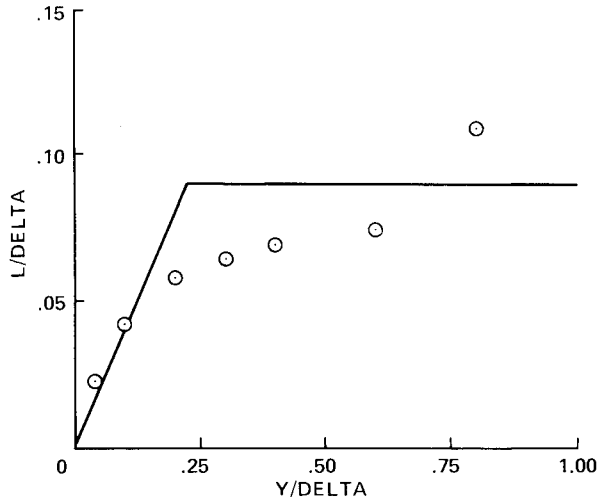

a) $x/c = -0.250$ and $\Delta = 1.270$ cm.

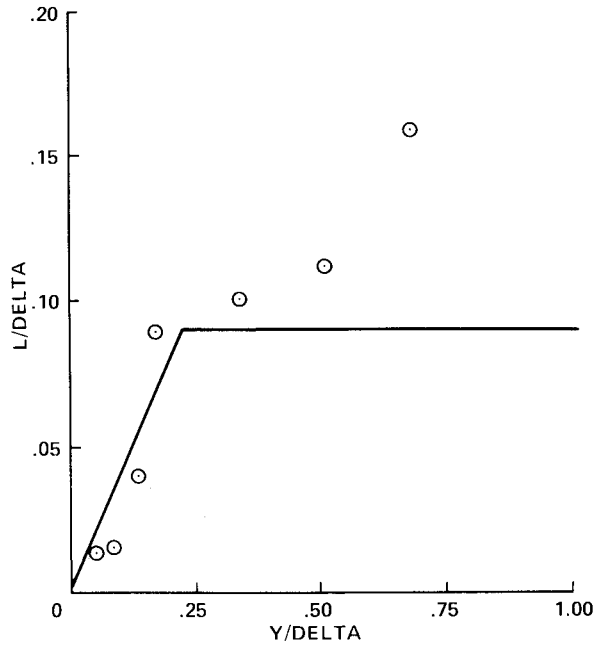

b) $x/c = 0.688$ and $\Delta = 1.500$ cm.

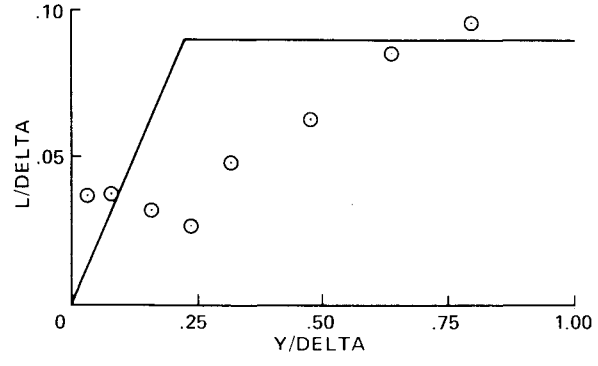

c) $x/c = 0.813$ and $\Delta = 1.600$ cm.

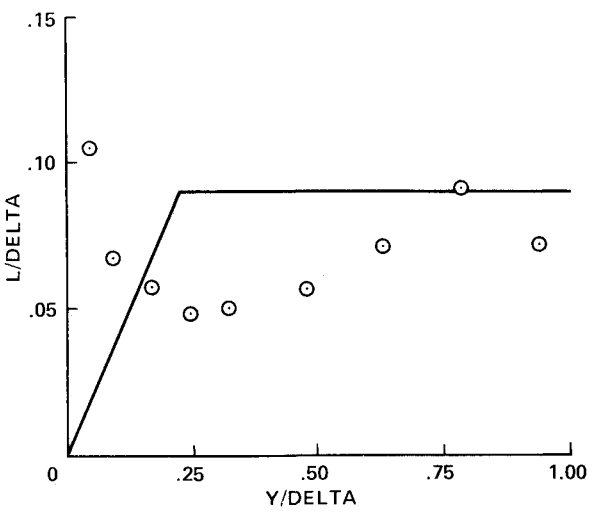

d) $x/c = 0.875$ and $\Delta = 1.650$ cm.

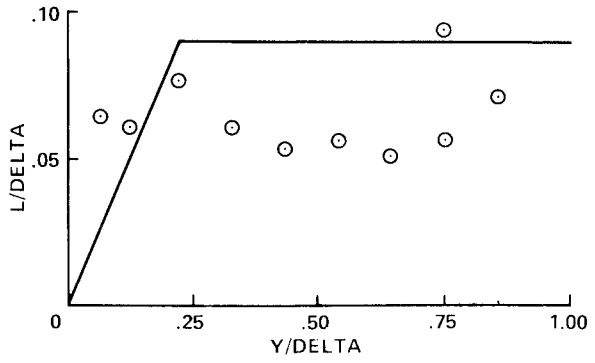

e) $x/c = 1.00$ and $\Delta = 2.400$ cm.

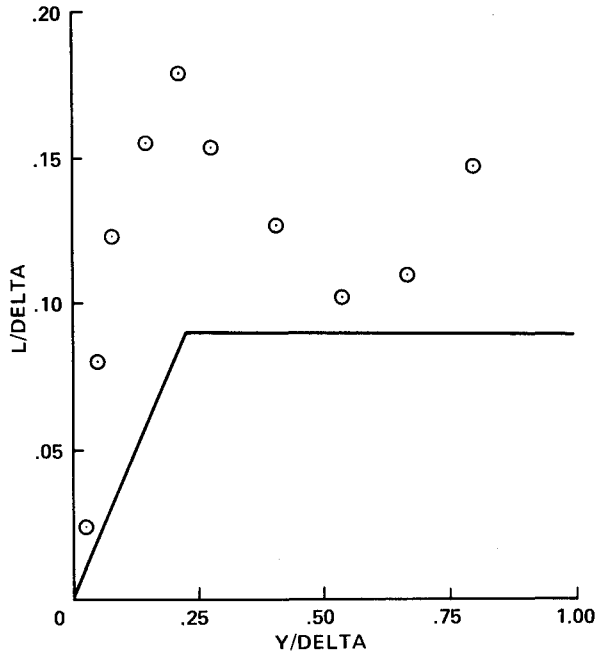

f) $x/c = 1.375$ and $\Delta = 1.950$ cm.

Fig. 12 Computed mixing-length distribution.

The slope of the model and the locations of the shock, separation, and reattachment are shown in the figure. These data show that upstream of the shock the flow gradually turned away from the wall at an angle of 2-3 deg. The continuous turning of the flow at the edge of the viscous layer throughout the interaction suggested that the inviscid flow near the model was turned by isentropic compression rather than by an oblique shock.

Separation occurred where the edge mean flow angle was approximately 4 deg measured with respect to the model surface. At separation, the flow angle was seen to turn away from the model in response to the sudden increase in the displacement thickness. Downstream of the separation point, the flow angle continued to decrease monotonically, and the relative angle between the model and the flow continued to increase. Beyond the model trailing edge, the flow angle increased as the flow in the boundary layer gained momentum. Note that the model slope changed discontinuously from -20.8 to 0 deg at the trailing edge of the bump.

Shear Stress and Mixing Length

The Reynolds shear-stress profiles were evaluated and the results are presented in Fig. 9. Assuming that the density fluctuations and mean density changes across the boundary layer were small, the shear stress was given by

$$\frac{\overline{\rho u' v'}}{\rho_e u_e^2} \approx \frac{\overline{u' v'}}{u_e^2} \tag{2}$$

Measurements of this flow property throughout the interaction, separation, and reattachment regions were of paramount importance to the development and evaluation of turbulence closure models.

In the neighborhood of the interaction, the upstream influence of the shock coupled with the shear forces imposed by the wall produced a deceleration of the flow in the low-momentum inner region of the boundary layer. Passage of the outer supersonic flow through the compression envelope apparently introduced a perturbation into the outer region of the boundary layer that manifested itself as an increase in the shear stress. Jitter in the compression fan induced by the turbulent fluctuations at the edge of the layer should be expected in all shock/turbulent boundary-layer interactions. The corresponding velocity correlation occurred as a result of the instantaneous fluctuations of the velocity vector with the fluctuating strength of the compression waves.

In the neighborhood of the separation line, the shear stress and shear-stress gradient in the wall region increased sharply. Continued deceleration of the flow in the wall region by the prevailing pressure forces displaced the flow with the strong velocity gradient outward and increased the magnitude of the velocity fluctuations. The maximum shear stress occurred at a height above the model surface that approximately corresponded to the center of the large boundary-layer gradient of the $\bar{u}$ profiles shown in Fig. 5.

An extreme value of the Reynolds shear stress of $\overline{u' v'}/u_e^2 \approx 0.16$ was reached at $x/c = 1.00$. The maximum shear-stress level at each measurement station was plotted (Fig. 10) to show its variation with streamwise distance. A steep increase in the shear stress was identified at the separation line. Thereafter, the shear continued to increase to a peak value in the neighborhood of reattachment. This maximum shear along with the large inner shear-stress gradient was sufficient to rehabilitate the separated flow. The shear stress then decreased at an exponential rate.

Turbulent energy production profiles given by

$$P = \frac{\overline{u' v'}}{u_\infty^2} \frac{\partial(\bar{u}/u_e)}{\partial(y/\delta)} \tag{3}$$

which were a measure of the interaction between the mean flow and the turbulence were plotted at representative streamwise locations; see Fig. 11. Curves were sketched through the data to aid in viewing the profiles.

The turbulence energy production increased over an order of magnitude near the wall in the neighborhood of separation. Downstream, the peak production levels decreased. At reattachment, the production was down to approximately 10% of the maximum value.

Since the mean velocity profiles showed regions of constant gradients, a point location of maximum gradient could not be identified. The maximum shear stress was typically centered over the region of the maximum velocity gradient. Because of this and the relatively good agreement of the calculated mixing lengths with the Escudier model found for the separated flows of Refs. 5 and 8, a similar calculation was carried out (Fig. 12). The dimensionless mixing length given by

$$\frac{\ell}{\delta} = -\left(\frac{\overline{u' v'}}{u_e^2}\right)^{1/2} \Big/ \frac{\partial(u/u_e)}{\partial(y/\delta)} \tag{4}$$

was also used to estimate the excursions of the flow from equilibrium conditions.

Upstream of the bump, $x/c = -0.25$, reasonably good agreement was found with the relationships $\ell/\delta = 0.4 y/\delta$ in the inner region and the value $\ell/\delta = 0.09$ in the outer region used in equilibrium boundary-layer calculations (Fig. 12a).

Immediately downstream of the shock, $x/c = 0.69$ (Fig. 12b), which was in close proximity to the separation line, the mixing-length distribution for the inner part of the boundary layer was interpreted as conforming to the von Kármán constant of 0.4. Unfortunately, upstream of the shock, the velocity gradients were too small to determine the inner-layer, mixing-length distribution to a sufficiently high degree of accuracy. Thus, it was not clear whether the apparent $k = 0.4$ value at $x/c = 0.69$ was a remnant of a region having $k = 0.4$ upstream of the shock. It was evident that the inner mixing-length distribution observed at $x/c = 0.69$ did not persist into the separated region. Instead, the shear stress near the wall was observed to decrease at a rate less rapid than the mean velocity gradient, owing to history effects. This resulted in the larger mixing lengths obtained near the surface.

In the downstream neighborhood of the separation line, $x/c = 0.81$ (Fig. 12c), the magnitude of ℓ/δ was much lower than the equilibrium value on the central part of the boundary layer, but exceeded the value in the inner region. Although the shear stress was increasing in this region, the velocity gradient in the boundary layer (Fig. 5) had increased more rapidly. Downstream of reattachment an approximately linear mixing-length distribution was observed, but with a k value considerably larger than 0.4.

In general, in the outer region the mixing length was significantly less than the 0.09 value at the streamwise stations where

$$\tau_{\max} = \frac{\overline{u' v'}}{u_{\infty_{\max}}^2}$$

was increasing and was larger than 0.09 downstream where $\tau_{\max}$ was decreasing. This trend in the outer value was attributed to the upstream flow history effects.

Comparisons of these data with numerical predictions are given in Ref. 10.

Conclusions

An investigation of transonic flow over an axisymmetric flow model was undertaken in order to obtain detailed experimental information on the fundamental mechanism of transonic, turbulent, boundary-layer separation. The model configuration designed for this investigation proved to be well suited for this task. Detailed measurements of the flowfield revealed that the flow was free from any three-

dimensional effects and the interaction was relatively steady.

In the shock/boundary-layer interaction region, the shock was shown to degenerate into a compression fan. The flow angle measurements revealed that the flow was continuously away from the wall as the displacement thickness increased. This turning of the flow increased markedly at the separation line. The slope of the displacement thickness contour and the values of the form parameter H at separation and reattachment agreed with the values stated in the literature.

Determination of the mixing length at stations throughout the interaction, separation, and reattachment indicated the relative excursions of the turbulence from equilibrium conditions. Comparisons of the mixing lengths evaluated from the experimental data to the values assumed to be representative of an equilibrium boundary layer were made. These results were estimated in an effort to evaluate the relative response of the different regions of the boundary layer to the prevailing conditions.

Additional experimentation on other interaction conditions and with some further refinements in the methods for observing the surface flow and measurements of the skin friction would be desirable.

References

[1]Rubesin, M. V., "Development in the Computation of Turbulent Boundary Layers," *Turbulent Boundary Layers, Experiments, Theory and Modelling*, Paper 11, AGARD CP 271, Sept. 1979.

[2]Alber, I. E., Bacon, J. W., Masson, B. S., and Collins, D. J., "An Experimental Investigation of Turbulent Transonic Viscous-Inviscid Interactions," *AIAA Journal*, Vol. 11, May 1975, pp. 620-627.

[3]Altstatt, M. C., "An Experimental and Analytical Investigation of a Transonic Shock-Wave Boundary Layer Interaction," AEDC TR 77-47, May 1977.

[4]Seegmiller, H. L., Marvin, J. G., and Levy, L. L., "Steady and Unsteady Transonic Flow," AIAA Paper 78-160, Jan. 1978.

[5]Johnson, D. A. and Bachalo, W. D., "Transonic Flow About a Two-Dimensional Airfoil—Inviscid and Turbulent Flow Properties," AIAA Paper 78-1117, July 1978.

[6]Bachalo, W. D., Modarress, D., and Johnson, D. A., "Experiments on Transonic and Supersonic Turbulent Boundary Layer Separation," AIAA Paper 77-47, Jan. 1977.

[7]Kline, S. J., Cantwell, B. J., and Lilley, G. M., eds., *Proceedings of the 1980-81 AFOSR-HTTM-Stanford Conference on Complex Turbulent Flows: Comparison of Computation and Experiment*, Case 8611, Stanford University, Stanford, CA, Sept. 1980.

[8]Johnson, D. A., Bachalo, W. D., and Owen, F. K., "Transonic Flow Past a Symmetrical Airfoil at High Angle of Attack," AIAA Paper 79-1500, July 1979.

[9]Alber, I. E., "Similar Solutions for a Family of Separated Turbulent Boundary Layers," AIAA Paper 71-203, 1971.

[10]Johnson, D. A., Horstman, C. C., and Bachalo, W. D., "Comparison Between Experiment and Prediction for Transonic Turbulent Separated Flow," *AIAA Journal*, Vol. 20, June 1982, pp. 737-744.